

L. Bitsch · L. H. Olesen · C. H. Westergaard
H. Bruus · H. Klank · J. P. Kutter

Micro particle-image velocimetry of bead suspensions and blood flows

Received: 17 July 2003 / Accepted: 30 July 2004 / Published online: 29 June 2005
© Springer-Verlag 2005

Abstract We present and discuss velocity profiles of microflows obtained by micro particle-image velocimetry in a transmission setup. We have measured suspensions of beads in water and on human blood, using the red blood cells as a natural particle seeding. The limitations imposed by our optical system on the spatial resolution normal to the focal plane, the so-called focal depth, have also been analyzed. The first direct observations of the influence of the focal depth on the observed velocity profiles are presented. Good agreement is obtained between observations and calculated profiles modified by the finite focal depth through a weight function.

Particular the non-linear flow properties of blood are interesting. To date, the studies of blood flow in microsystems presented in the literature often focus on measurements and models of the relation between flow rates and pressure drops (Trebotech et al. 2001), without utilizing the support of PIV. One exception is Sugii et al. (2002) who presented an in vivo PIV experiment of blood flow. However, they did not investigate the influence of velocity gradients normal to the focal plane, and such an investigation is generally needed. Furthermore, the measurements were not compared to theoretical profiles. Therefore, the paper presented here is the first to directly compare the shape of experimental and theoretical profiles.

In this work, using μ PIV in a transmission setup, we measure velocity profiles of bead suspensions and blood flows in a flat glass capillary with a roughly rectangular cross-section of size $28\ \mu\text{m}$ by $360\ \mu\text{m}$. Restricted to observations in a given focal plane μ PIV has previously proven successful in both transmission and epi-fluorescent mode (Koutsiaris et al. 1999; Meinhart et al. 1999). We extend these results by taking into account the finite spatial resolution normal to the focal plane, the so-called focal depth, imposed by our optical system, and we present the first direct observation of the influence of the focal depth on the obtained experimental velocity profiles. Our analysis is inspired by the theoretical expression for the visibility of particles slightly out-of-focus that has recently been derived by Olsen and Adrian (2000). For fluids with a high particle density, such as blood, it can be difficult to determine the position of boundaries parallel to the focal plane. We show that these boundaries are related to a steep increase in the size of the error bars of the measurements. The blood measurements strongly indicate that blood in these dimensions flows as a plug flow and that it should be modeled as a two-phase flow. Moreover, we find indications of the presence of a $3\text{-}\mu\text{m}$ wide cell-free boundary layer.

The paper is organized as follows. In Sect. 2 we describe the bead suspensions and blood samples used in

1 Introduction

The efforts to develop lab-on-a-chip devices have increased substantially during the past few years (Sanders and Manz 2000). Along with this development the techniques to characterize the performance of microfluidic systems are being improved drastically. Volume illuminated micro particle-image velocimetry (μ PIV) has shown to be a promising technique for characterizing detailed velocity profiles in these structures.

An important sub-field in microfluidics concerns the behavior of blood flowing in microchannels, and it has therefore become of high interest to obtain detailed information about the properties of such flows. In par-

L. Bitsch (✉) · L. H. Olesen · H. Bruus · H. Klank · J. P. Kutter
MIC—Department of Micro and Nanotechnology,
Technical University of Denmark,
2800 Kongens Lyngby, Denmark
E-mail: lbi@mic.dtu.dk
Tel.: +45-4525-5742

C. H. Westergaard
Dantec Dynamics A/S, Tonsbakken 16-18,
2740 Skovlunde, Denmark

our experiments, with special attention to the non-linear flow properties of the latter. In Sect. 3 we present the details of our μ PIV setup. The central concept of focal depth is explained in Sect. 4. Section 5 contains a description of the μ PIV data analysis. In Sect. 6, based on the finite focal depth, we derive the theoretical expression for the convolved velocity field. Our results are presented and discussed in Sect. 7, and followed by a summary in Sect. 8.

2 Preparation of samples

For the measurements we used human blood delivered from the hospital blood bank at Rigshospitalet, Copenhagen (Rigshospitalet 2003). More precisely, the blood was a suspension of red blood cells in an aqueous solution of adenine, mannitol, sodium chloride, and glucose. The role of the suspending medium is to serve as an energy source for the biochemical processes in the red blood cells and to prevent coagulation and hemolysis. However, since in this work we are mostly interested in the non-linear flow properties of blood, and since a major cause of this non-linearity is the deformation and flow alignment of the red blood cells (Fung 1993), we expect a good resemblance between our blood samples and anticoagulated whole human blood. The blood was stored at 4°C before use, but all experiments were conducted at room temperature, 20°C.

The non-linear flow properties of blood are clearly seen in its viscosity. It is more pronounced at high concentrations of red blood cells, and for that reason we chose to work with the undiluted suspension with a hematocrit at about 60%, whereas a normal human hematocrit is about 50% depending on gender and physical condition. The typical diameter of a red blood cell is approximately 8 μm . In Fig. 1 the viscosity η of a

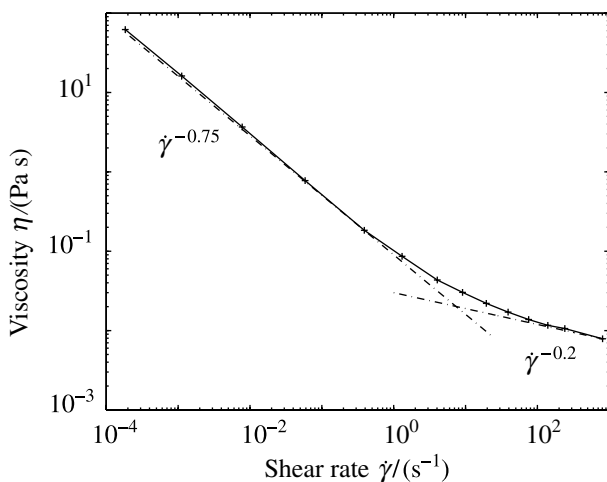


Fig. 1 The viscosity of blood as a function of shear rate obtained in a concentric cylinder geometry. With its shear rate dependent viscosity, blood is clearly a non-Newtonian fluid. The *straight lines* indicate the different power laws at high and low shear rates

blood sample is shown as a function of the shear rate $\dot{\gamma}$. The viscosity measurements were conducted with a rotational rheometer (AR 2000 Advanced Rheometer, TA instruments, Delaware, USA). The viscosity shows a strong dependency on the shear rate in agreement with other studies of blood (Fung 1993). Instead of a constant η characteristic for a Newtonian liquid, we see that blood for low shear rates follows a power law $\eta \propto \dot{\gamma}^{-0.75}$, which then tapers off at higher shear rates, $\eta \propto \dot{\gamma}^{-0.2}$.

As the blood sample had a tendency to develop a sticky skin when exposed to air, we chose to use a concentric cylinder geometry, where a relatively large sample volume minimizes the influence of a skin. The distance between the two cylinders was 1 mm, and the measured viscosity is therefore a bulk property. The viscosity will vary between individual blood donors. However, since we use the measured blood viscosity for a qualitative estimate of the suitability of a bulk property model, we are not concerned with such variations, but instead only focus on the qualitative behavior.

As a reference fluid to blood we chose to work with a suspension of spherical beads in pure water. The bead seeding was about 1–3% by volume, and each bead had a diameter of 1.02 μm . The measured viscosity of the bead suspension was 7% larger than the viscosity of pure water, and, most importantly, no shear rate dependency was observed. Einstein's prediction for the viscosity of a dilute suspension of small particles states an increase of 3%. However, the uncertainty of the measured volume fraction may explain the deviation, and moreover Einstein's formula is believed to be valid for volume fractions below 2% (Batchelor 2000).

3 The measurement setup for IPIV

The measurement setup for μ PIV is sketched in Fig. 2a. It is centered around an optical microscope (Leica DMLB, GTI Microsystems, Tempe, Arizona) using a CCD camera to record images of the flow of blood or bead suspensions through the capillary. The capillary is placed horizontally in the microscope and illuminated from below by a high intensity light-emitting diode (LED) with a maximum intensity at a wavelength of 450 nm. The transmitted light is focused onto a CCD-camera by a dry infinity-corrected PI fluotar objective lens with a magnification of 63 and a numerical aperture of 0.7. Camera and LED were synchronized and controlled by a FlowMap System Hub from Dantec Dynamics (Bristol, UK).

The CCD-camera is a PCO SensiCam with a 12 bit cooled imaging system containing a matrix of 1,280×1,024 pixels. By calibration in air this matrix was found to correspond to a field of view of 129×103 μm^2 .

A cross section of the capillary is seen in Fig. 2b. During experiments it was filled with the fluid from a syringe pump through approximately 20 cm long PVC tubes. After passing the capillary, the fluid ended up in a waste beaker at atmospheric pressure. The flow rates

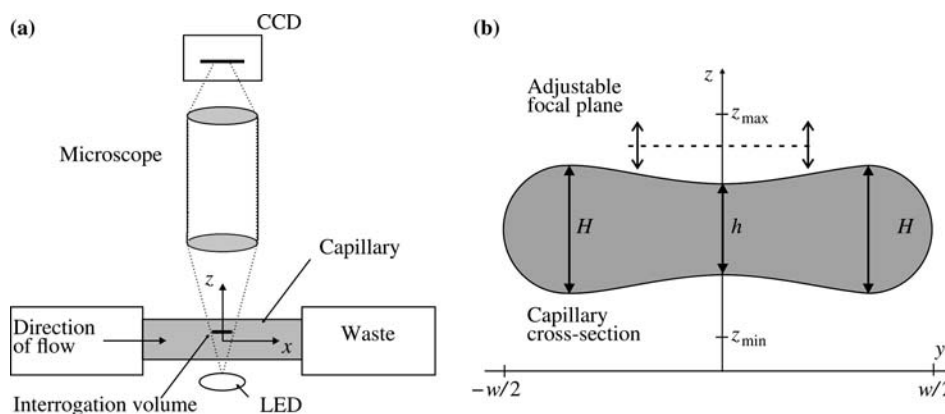


Fig. 2 (a) A sketch of the experimental setup containing the microfluidic system, the interrogation volume, the LED, the optical system, and the CCD camera. (b) The actual channel cross section in the yz plane obtained by optical inspection. The dimensions are $H = 32.5 \mu\text{m}$, $h = 28 \mu\text{m}$ and $w = 360 \mu\text{m}$ (not drawn to scale). The z -axis is normal to the focal plane. The velocity profiles were

were 50 nL s^{-1} for the bead suspension and 167 nL s^{-1} for blood.

An experiment consisted of a series of PIV measurements, where the horizontal focal plane was moved vertically down through the channel, as sketched in Fig. 2b. In that way the velocity gradient could be resolved in the direction normal to the focal plane.

A PIV measurement consisted of 25 pairs of images recorded with intervals of 1 s. The time lapse between the two images in a pair was $500 \mu\text{s}$, and the exposure time for each single image was given by the $100 \mu\text{s}$ LED pulses. The exposure time and time between pulses were adjusted in such a way that a reasonable signal to noise ratio was obtained on the measured velocities. To minimize the uncertainty on the traveled distance, the ratio between the exposure time and time between pulses should be as small as possible. We have not optimized this procedure in a systematic way, but rather used a rough guideline that requires a movement of 10 pixels between subsequent exposures and a ratio of 5 for time between pulses and exposure time. A general rule of thumb in PIV says the ratio must be approximately 10 or higher. However, we had a practical trade-off given the maximum illumination intensity available and the flow rate. Direct image blur was not seen.

From each pulse pair an instantaneous velocity field of the particle images could be calculated. As an example the velocity field for a blood flow measurement is seen in Fig. 3. Since we were studying steady-state flow the velocity field was constant, and 25 sets of images were recorded and used to present an averaged result with improved statistics.

4 Focal depth and focal plane

The spatial resolution normal to the focal plane, the so-called focal depth D_f , was estimated experimentally to be

$4 \mu\text{m}$. Here D_f is defined as the full-width at half-maximum in a plot of the recorded gray-scale values of a given bead at the bottom of a water-filled channel as a function of the vertical position of the horizontal focal plane (Fig. 4). The measured gray-scale signal (inverse intensity) is seen to be superimposed on a flat background without any refraction patterns. This background is indicated by the lower dotted line.

To minimize effects from out-of-focus particles we use a so-called base-clipping technique. A specific gray-scale threshold level is chosen (the upper dotted line in Fig. 4) and gray-scale values below this level are discarded. In this specific case, base-clipping discards all patterns with a gray-scale value corresponding to a distance further than $1.25 \mu\text{m}$ away from the focal plane. In other cases, different distances can be observed.

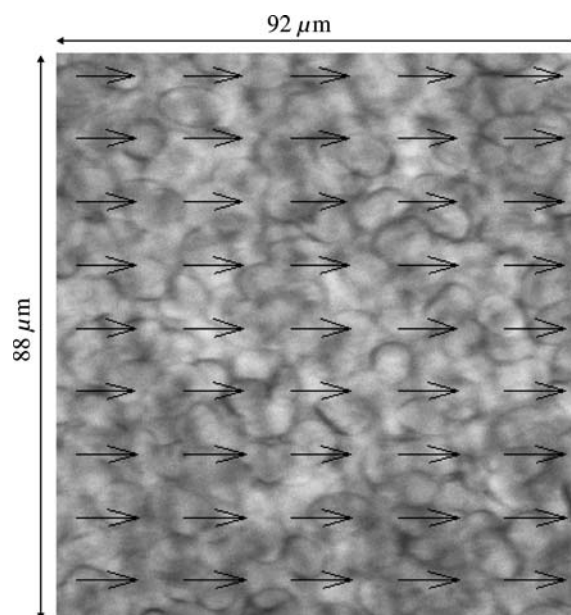


Fig. 3 An example of a velocity field obtained for a flow measurement of blood. The map is $92 \mu\text{m}$ wide and $88 \mu\text{m}$ high. The blood cells are observed as dark rings, and the average velocity of some interrogation areas are indicated with an *arrow*. The velocity is approximately 16 mm s^{-1} , and the image is obtained $5 \mu\text{m}$ below the top of the channel

The optical effects of changing the position of the focal plane need special attention. The change Δz_{fp} in vertical position of the focal plane relative to the capillary is obtained by moving the objective table with the capillary a distance Δz_{cap} in steps of $1 \mu\text{m}$ using the built-in scale on the microscope. In air we simply have $\Delta z_{fp} = \Delta z_{cap}$, but in the fluid the light rays are bent away from the vertical direction by refraction. Using the theory of paraxial rays we find the linear scaling

$$\Delta z_{fp} = \frac{n_{\text{water}}}{n_{\text{air}}} \Delta z_{cap} \quad (1)$$

where $n_{\text{water}} = 1.33$ and $n_{\text{air}} = 1$ are the refractive indices of water and air, respectively.

5 IPIV data analysis

Data were analyzed using standard PIV-analysis (Dantec Dynamics 2005). Typically in PIV an illuminated volume is projected onto a plane, i.e., a particle image is produced on a CCD-chip. In order to obtain a velocity field the image is divided into smaller areas called interrogation areas. The density of particles or, more precisely, the density of refraction patterns determines the minimum resolution within the image plane. The resolution normal to the focal plane is dependent on the focal depth D_f after base-clipping. The interrogation area combined with D_f is, therefore, a reasonable estimate of the interrogation volume.

A rule of thumb requires approximately ten particles per interrogation volume to enable so-called ordinary cross-correlation analysis. A particle suspension of 1% by volume, and an interrogation volume given by

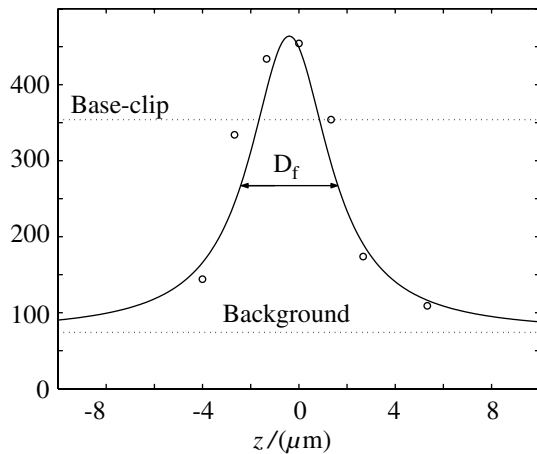


Fig. 4 The recorded gray-scale values (*open circles*) in arbitrary units of a given bead in a water-filled capillary as a function of the vertical distance z from the horizontal focal plane. High gray-scale values correspond to low light intensities and vice versa. The full line is a fit to a Lorentzian profile. The full-width at half-maximum is $4 \mu\text{m}$, which defines the focal depth D_f . The *upper* and *lower dotted horizontal lines* are the base-clipping level and background level, respectively. In this particular case, the base-clipping level corresponds to a distance of $1.25 \mu\text{m}$ away from the focal plane

$6.4 \times 6.4 \times 4 \mu\text{m}^3$ corresponds roughly to 2.4 spherical particles. Hence, our particle seeding was a little too low, but we can compensate for this problem by making an average correlation, as explained below. In order to improve the spatial resolution we used a 25% overlap between the interrogation areas.

The recorded light intensity I (in reality recorded as gray-scale values) in a given interrogation area can, without going into details, be written as a function of the pixel position vector \mathbf{s} as $I_1(\mathbf{s})$ and $I_2(\mathbf{s})$ for the two light pulses at time t_1 and t_2 , respectively. The cross-correlation function $R(\Delta\mathbf{x})$ is defined as the average over all pixel coordinates in the interrogation area I as

$$R_i(\Delta\mathbf{x}) \equiv \langle I_1(\mathbf{s})I_2(\mathbf{s} + \Delta\mathbf{x}) \rangle_I \quad (2)$$

The value $\Delta\mathbf{x}_I$ of $\Delta\mathbf{x}$ that maximizes $R_I(\Delta\mathbf{x})$ is a statistical measure of the overall displacement of the fluid represented by the interrogation area. Thus the average flow velocity of that region is given by

$$\mathbf{v}_I = \frac{\Delta\mathbf{x}_I}{t_2 - t_1}. \quad (3)$$

From each set of particle images we can, in principle, determine the velocity field. However, a better approach is to compute the average correlation function over all 25 images for each individual interrogation area, and then derive the velocity. With 25 images and 2.4 particles per interrogation volume we improve the confidence and accuracy for individual velocity measurements, simply because we have approximately 60 independent particles contributing to the correlation. The result with 25 images is a vector confidence quite similar to the one obtained with one image in normal PIV realization (rule of thumb in normal PIV: interrogation areas should hold six to ten particles or more). With more images the confidence and accuracy could be improved further, if required. The procedure is widely used in microfluidics and is often called average correlation or ensemble correlation.

6 Theoretical velocity fields

The measured velocity fields from the μPIV analysis need to be compared with theoretical velocity fields. These are found by solving the Navier–Stokes equation with a constant negative pressure gradient along the flow direction and with the no-slip boundary conditions for the velocity at the channel walls.

For the bead suspension, being a Newtonian liquid, the calculated Navier–Stokes velocity field v_{NS} can be thought of as the well-known paraboloid Poiseuille profile being distorted at the boundary to fit the dumbbell shape depicted in Fig. 2b rather than a circular shape.

Due to the small height to width aspect ratio and the almost rectangular channel shape, the analytical solution for a flow between two infinite planes describes the

fluid velocity, i.e., the flow profile is parabolic. The maximum velocity of the theoretical velocity profile was then fitted to the maximum velocity of the PIV-measurements.

The non-Newtonian character of blood, as seen in Fig. 1, leads to a further distortion of the Poiseuille flow in the form of a more blunt velocity profile close to the center of the capillary. Due to the small dimension of the channel compared to the size of the red blood cells, another option is to model the fluid as a two-phase system.

However, in our μ PIV experiments we expect to observe neither of these two simple Navier-Stokes velocity fields. Even though we have performed a truncation in gray-scale levels, the remaining optical depth of our system will cause a pick-up of out-of-focus signals. Recently, Olsen and Adrian (2000) derived a theoretical expression for the visibility of particles slightly out-of-focus, which in a particularly simple limiting case is a Lorentzian. Inspired by this, we model our observed gray-scale function as the following Lorentzian shape,

$$W(z) = \left(1 + \frac{4z^2}{D_f^2}\right)^{-1}. \quad (4)$$

Using $W(z)$ as a weight function we can model the observed smearing of the velocity field induced by the finite focal depth D_f . This is done by the following convolution integral $v_{\text{conv}}(z)$ of the simple theoretical velocity field $v_{\text{NS}}(z)$:

$$v_{\text{conv}}(z) = \frac{\int_{-h/2}^{h/2} v_{\text{NS}}(z')W(z' - z)dz'}{\int_{-h/2}^{h/2} W(z' - z)dz'}. \quad (5)$$

where h is the height of the channel.

A theoretical estimate of the error bars $\sigma_v(z)$ can be obtained as being inversely proportional to the square root of the amount of statistical data,

$$\sigma_v(z) \propto \left[\int_{-h/2}^{h/2} W(z' - z)dz' \right]^{-1/2}. \quad (6)$$

It is important to notice that we cannot expect total agreement between $v_{\text{conv}}(z)$ and the measured velocity $v_{\text{PIV}}(z)$. $v_{\text{conv}}(z)$ is the weighted average of a theoretical profile, where the weight function $W(z)$ is given by Eq. 4, and no base-clipping is considered. v_{PIV} is based on measured data after base-clipping, which reduces the signal from out-of-focus particles. Despite the base-clipping there still is some influence from the finite optical resolution due to varying background levels. We estimate it qualitatively by means of a convolution.

For the PIV measurements, it was not possible to obtain a measurement for the distance which corresponded to the level of base-clipping. In Fig. 4 this distance was estimated to 1.25 μm in a separate experi-

ment, and for a fixed base clipping level this distance will change with the level of the background signal. In the PIV-measurements the background level was slightly higher, and the base-clip is, therefore, believed to be below the half maximum level.

7 Results and discussion

As a first result, Fig. 5a contains a comparison of two experimental velocity profiles $v_{\text{PIV}}(z)$ with the simple theoretical profile $v_{\text{NS}}(z)$ for the suspension of beads in water. The theoretical velocities are fitted to the measured around the center, but a discrepancy is observed closer to the boundaries. Beyond the boundaries, an out-of-focus signal is picked up, a feature which is not captured at all by the simple theoretical profile. However, the effect is real, and is nicely reproduced in the two different experiments.

Using instead the weighed theoretical profile $v_{\text{conv}}(z)$ from Eq. 5 we obtain Fig. 5b, where it is seen that the convolution with the weighing function yields a qualitatively correct description of the non-zero values at the channel boundaries. It furthermore explains both the increase in the observed velocities outside the channel, and the rapid increase in uncertainty.

Our measurements on the beads demonstrate that it is possible to resolve velocities normal to the focal plane with a focal depth of $\sim 4 \mu\text{m}$ using volume illuminated μ PIV, averaged cross-correlation and base-clipping.

We have seen that moving the focal plane outside the channel leads to an increase in observed velocities and to a steep increase in the associated uncertainties. This can be explained qualitatively as follows. When the focal plane and hence the maximum of the visibility function lies outside the channel, the observed average velocity increases because the high-velocity particles in the center of the channel are seen with the same low gray-scale value as the low-velocity particles at the boundaries. Moreover, only very few particles are observed at all thus resulting in large $1/\sqrt{N}$ -fluctuations and increased uncertainties.

As it was difficult to measure the exact geometry of the channel cross section, it was chosen not to perform a numerical simulation. However, approximating the cross section with a rectangle of $28 \times 360 \mu\text{m}^2$ yields a mean velocity of 4.96 mm s^{-1} , which is a reasonable value.

For the blood measurements, the velocity profile is seen in Fig. 6a with the corresponding uncertainties. The uncertainty of a velocity measurement depends on the density of the moving refraction patterns (the image density) in the interrogation volume. For positions of the focal plane inside the blood-filled channel, the particle seeding is relatively high, and the uncertainties become correspondingly small. Even outside the channel the uncertainties are surprisingly small, but as in the

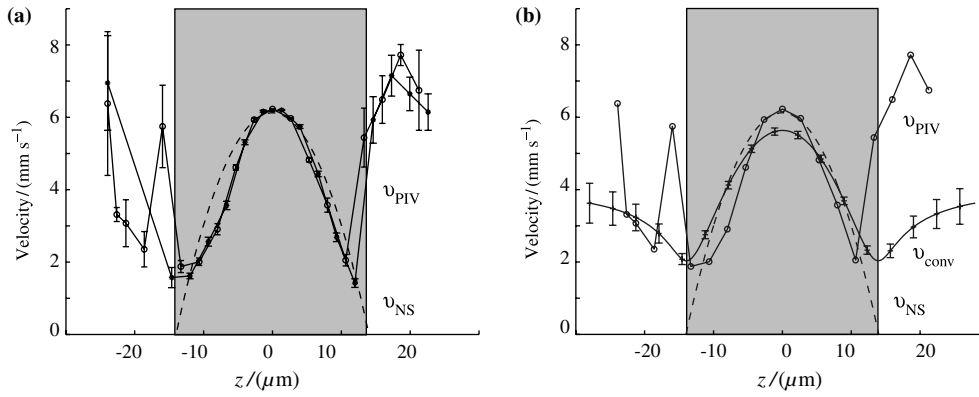
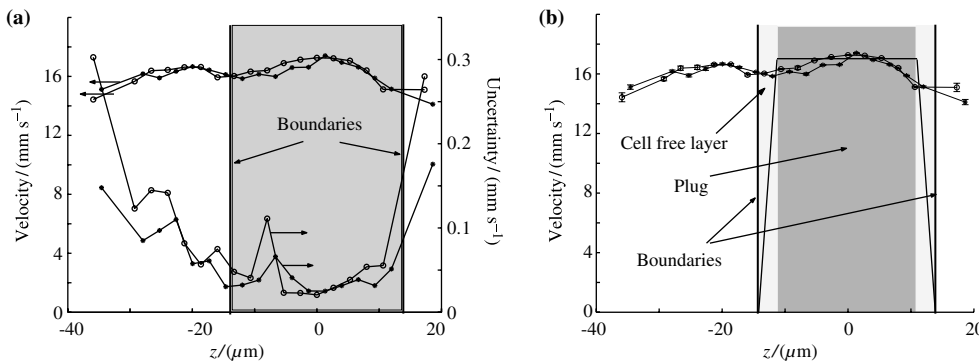


Fig. 5 The velocity of the bead suspension versus z . The channel position is indicated with *gray background*. (a) The z -axis has been centered around the middle of the channel. Legends: *continuous line with open circle* first experiment v_{PIV} , *continuous line with asterisk* second experiment v_{PIV} , and *broken line* Navier-Stokes theory $v_{NS}(z)$. Experimental uncertainties are indicated with *error bars*. (b) The weighed theoretical profile $v_{conv}(z)$ obtained from a convolution of the Navier-Stokes profile $v_{NS}(z)$ with the weighing function $W(z)$ of Eq. 4 and Fig. 4. Legends: *continuous line* theory $v_{conv}(z)$, a *broken line* theory $v_{NS}(z)$, and *continuous line with open circle* first experiment v_{PIV} . Theoretical uncertainties are

case of the bead suspension they increase significantly as the focal plane is moved outside the channel. The first channel wall was positioned where the steepest increase in uncertainty was observed (bottom), and the second wall (top) was determined by the channel height.

Blood is known to develop cell-free layers next to solid boundaries to lubricate the transport of a semi-solid plug consisting of cells (Fung 1993), i.e., a two-

Fig. 6 Measurements on blood flows. (a) The velocity (*upper curves*) and the uncertainty (*lower curves*) as a function of z . The z -axis has been centered around the middle of the channel. The channel boundaries (*top and bottom*) are indicated by *vertical lines* at $z = \pm 14 \mu\text{m}$. Legend: *continuous line with open circle* first experiment, *continuous line with asterisk* second experiment. The uncertainty increases strongly outside the boundaries. (b) A comparison between the suggested two-phase model and the experimental results. Legend: *continuous line* two-phase model, *continuous line with open circle* first experiment, *continuous line with asterisk* second experiment



phase system. The nearly flat velocity profile in Fig. 6a strongly suggests that such a two-phase model indeed is a good description of the system, whereas a single-phase model employing the viscosity data from Fig. 1 does not fit the data. A two-phase model is seen in Fig. 6b, where the velocity of the plug is 17 mm s^{-1} , and the cell-free layer is a Newtonian liquid approximated with the viscosity of water, i.e., this assumption allows an analytical solution. We can obtain an estimate of the width d of the cell-free layer by matching the nominal flow rate Q with the model. We find

$$d = 2 \left(A - \frac{Q}{v_0} \right) \frac{1}{l}, \quad (7)$$

where $A = 1.09 \times 10^{-8} \text{ m}^2$ is the area of the channel, $Q = 1.67 \times 10^{-10} \text{ m}^3 \text{ s}^{-1}$, $v_0 = 17 \times 10^{-3} \text{ m s}^{-1}$ is the plug velocity, and $l = 7.57 \times 10^{-4} \text{ m}$ is the perimeter of the channel. The cell-free layer was calculated to be $d = 3 \mu\text{m}$, which is 21% of the channel. In the literature it is reported that cell-free layers in microtubes for diluted blood samples took up to about 10% of the volume (Fung 1993). Considering the increase in uncertainties and the fine agreement with the two-phase model, it is reasonable to assume that we have been able to resolve the velocities along the z -axis, and that we have observed a plug flow. However, the discrepancy between theoretical and experimental velocities in the cell-free layer should not be ignored. It illustrates the challenges to the optical system, and this experiment is only an indirect measurement of a cell-free layer.

8 Summary

We have successfully measured steady-state velocity profiles on suspensions of beads and human blood in a microchannel. The microflows were imaged through an optical system using stroboscopic back illumination. Due to the focal depth, the optical system limits the resolution vertical to the focal plane, which results in an averaging of velocities in adjacent planes. In the bead suspension, we have qualitatively estimated the influence of the focal depth by means of a Lorentzian weight function (Eq.14). Using this weight function, we show that the optical system has a focal depth of 4 μm . Furthermore, the weight functions illustrate why the measured velocity seems to increase when the focal plane is moved outside the fluidic channel. Additionally, it provides a prediction of the trend in uncertainties, which can be a help in determining the position of walls parallel to the focal plane.

In the blood suspension we measured a velocity profile which, together with a two-phase model, gives a strong indication of a plug flow. The fitting of a two-phase model resulted in a cell-free layer of 3 μm .

Acknowledgements The authors thank Detlef Snakenborg from MIC for providing the electronic circuitry to help in controlling the LED, and the Polymer Center at DTU for making it possible to perform the viscosity measurements. This work was supported by

the Danish Technical Research Council, μTAS Frame Program Grant No. 26-00-0220.

References

- Batchelor GK (2000) An introduction to fluid dynamics. Cambridge University Press, London
- Dantec Dynamics (2005) FlowManager version 3.70.06. Dantec Dynamics A/S, Skovlunde, Denmark
- Fung YC (1993) Biomechanics, 2nd edn. Springer, Berlin Heidelberg New York
- Koutsiaris AG, Mathioulakis KS, Tsangaris S (1999) Microscope PIV for velocity-field measurement of particle suspensions flowing inside glass capillaries. *Meas Sci Technol* 10:1037–1046
- Meinhart CD, Wereley ST, Santiago JG (1999) PIV measurements of a microchannel flow. *Exp Fluids* 27:414–419
- Olsen MG, Adrian RJ (2000) Out-of-focus effects on particle image visibility and correlation in microscopic particle image velocimetry. *Exp Fluids* 29:S166–S174
- Rigshospitalet (2003) Blodbank. H:S Rigshospitalet, Copenhagen, Denmark
- Sanders GHW, Manz A (2000) Chip-based microsystems for genomic and proteomic analysis. *Trends Anal Chem* 19:364–378
- Sugii Y, Nishio S, Okamoto K (2002) In vivo PIV measurements of red blood cell velocity field in microvessels considering mesentery motion. *Physiol Meas* 23:403–416
- Trebotich D, Chang W, Liepmann D (2001) Modeling of blood flow in simple microchannels. In: *Proceedings of the modeling and simulation of microsystems 2001*, Hilton Head, SC, 19–21 March 2001, pp 218–222